

High speed video capture for mobile phone cameras

with Analog Devices

Technical Report from MACSI's 2012 Problem-Solving Workshop
with Industry

Report MACSI/ESGI/0031



Mathematics Applications
Consortium for Science
& Industry



www.macsi.ul.ie
00353 (0)61 213013

High speed video capture for mobile phone cameras

M. Burke¹, S. Burns², S. P. Cook³, P. J. Dellar⁴,
J. Dewynne⁴, C. Hickey⁵, P. G. Hjorth⁶, W. T. Lee⁷,
A. V. Melnik⁴, K. Moroney¹, E. Murphy⁷, R. O'Callaghan¹,
M. Vynnycky^{7,*}

¹Department of Mathematics and Statistics, University of Limerick,
Limerick, Republic of Ireland

²School of Mathematics, Statistics and Applied Mathematics,
NUI Galway, Galway, Republic of Ireland

³Department of Mathematical Sciences, University of Bath,
Claverton Down, Bath, BA2 7AY, United Kingdom

⁴Oxford University, Mathematical Institute, 24-29 St. Giles',
Oxford, OX1 3LB, United Kingdom

University College, Dublin, Republic of Ireland

⁶Department of Mathematics, Technical University of Denmark,
DK-2800 Kgs. Lyngby, Denmark

⁷Mathematical Applications Consortium for Science and Industry (MACSI),
Department of Mathematics and Statistics, University of Limerick,
Limerick, Republic of Ireland

*Corresponding author. E-mail: michael.vynnycky@ul.ie (Michael Vynnycky)

July 27, 2012

Abstract

We consider an electromechanical model for the operation of a voice coil motor in a mobile phone camera, with the aim of optimizing how a lens can be moved to a desired focusing motion. Although a methodology is developed for optimizing lens shift, there is some concern about the experimentally-determined model parameters that are at our disposal. Central to the model is the value of the estimated magnetic force constant, K_f : its value determines how far it is actually possible to move lens, but it appears that, from the value given, it would not be possible to shift the lens through the displacements desired. Furthermore, earlier experiments have also estimated the value of the back EMF constant, K_g , to be roughly five times greater than K_f , even though we present two theoretical arguments that show that $K_f = K_g$: a conclusion supported by readily-available manufacturers' data .

1 Introduction

Analog Devices manufacture control circuitry for focussing high speed cameras used in, for example, mobile phones; for relevant references on this topic, see [2,4–7]. In such a camera, the lens is mounted on a coil in series with a spring, and this entire assembly is housed within a magnet, as shown in Fig. 1. The system seeks a focussing position by moving the lens through a series of steps, achieved by passing a current through the coil; in the absence of an electrical current through the coil, the spring keeps the lens pressed against its housing. The lens assembly acts as a weakly damped oscillator, which leads to a phenomenon known as ringing, as shown in Fig. 2: in response to a current step, for example, the lens displacement oscillates slowly towards a desired steady position, resulting in poor image quality, slow auto focus, battery wastage and user frustration. This situation can be remedied by using a special current-time pulse to reduce oscillations, also shown in Fig. 2; however, this is not as effective when the lens makes contact with its housing - at this point, the force-displacement curve becomes highly nonlinear. This is demonstrated via Fig. 3, which demonstrates how the lens displacement varies linearly with the applied electric current (given on the horizontal axis) when the lens is not in the vicinity of the housing, but non-linearly when the lens is in the vicinity of either the top or bottom of the housing. A further complication is that the displacement response varies from phone to phone

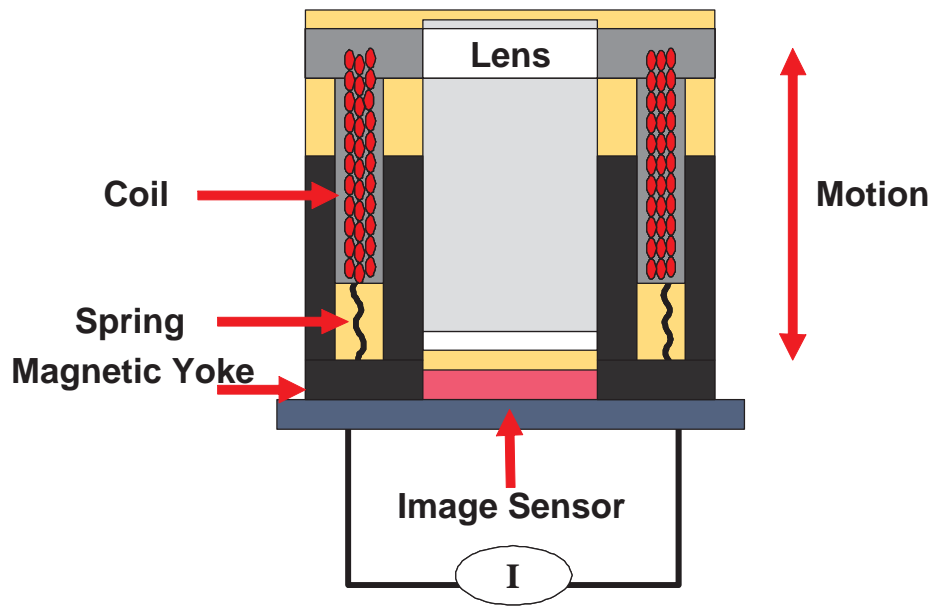


Figure 1: Voice coil motor

and with the orientation of the phone; from Fig. 3, it is evident that a greater current is necessary to displace the lens when the camera faces away from Earth than when it faces towards Earth. The specifications are that, irrespective of phone or angle of orientation and starting from any arbitrary position:

- it is possible to displace the lens to any other position within 10^{-2} s;
- the current used in doing so is no greater than 0.1 A;
- the maximum displacement necessary is $250 \mu\text{m}$ (although could be as high as $350 \mu\text{m}$, as suggested by Fig. 3);
- within the linear regime, any oscillations in the displacement should settle within 5 ms and to a tolerance of $1 \mu\text{m}$;
- within the nonlinear regime, any oscillations in the displacement should settle within 8 ms and to a tolerance of $1 \mu\text{m}$.

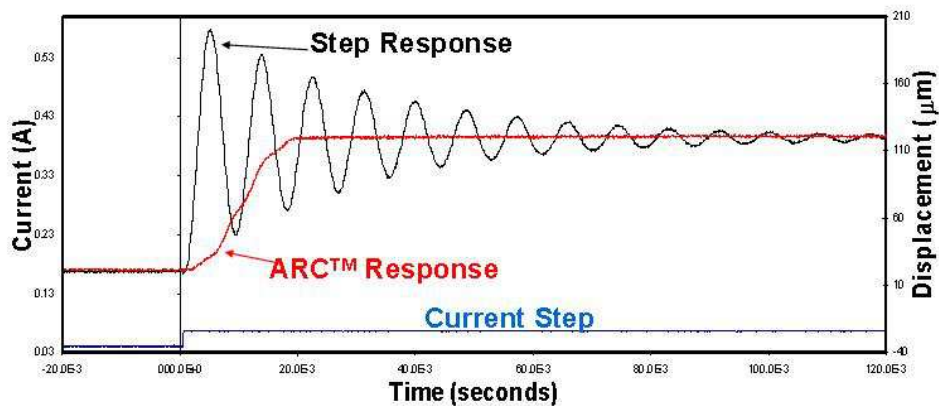


Figure 2: Displacement response to a current step, leading to ringing, and an improved strategy (ARC™) that eliminates ringing.

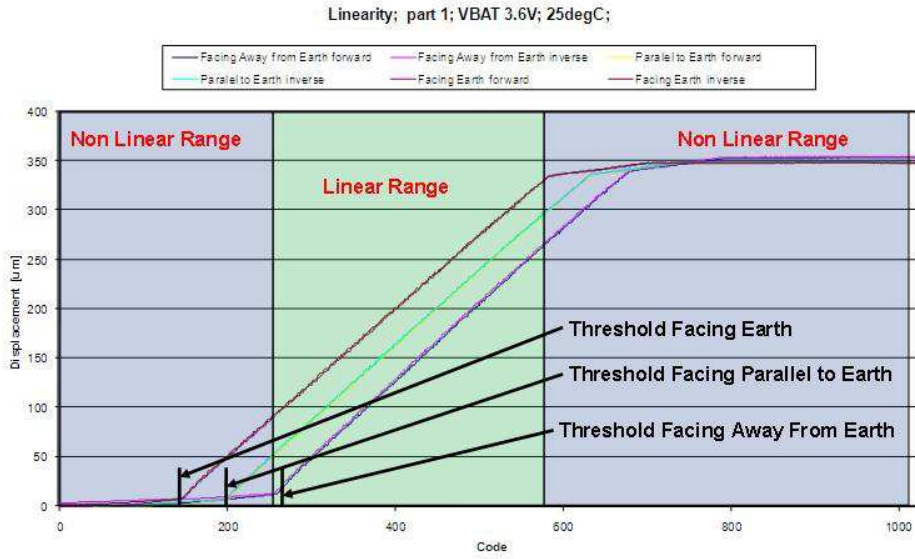


Figure 3: Experimentally determined lens displacement as a function of the applied current

With a view to engineering a current response that optimizes lens displacement, this report considers an electromechanical model for the system. Model equations are presented in §2, and nondimensionalized in §3, with preliminary results being given in §4. In §5, conclusions are drawn and recommendations for future work are outlined.

2 Modelling

The model presented is concerned primarily with the so-called “linear regime” where the pre-stress in the spring has been overcome and it is also assumed that a change in the current applied to the coil results in an immediate (and linear) change in the force applied by the magnetic field.

The system is governed by: the force balance equation,

$$m \frac{dx^2}{dt^2} + B \frac{dx}{dt} + kx = K_f I, \quad (2.1)$$

where x is the displacement of the lens, t is the time, I is the applied current, m is the mass of the lens, B is the drag coefficient, k is the spring stiffness and K_f is the magnetic force constant; and the circuit equation,

$$V = IR + L \frac{dI}{dt} + K_g \frac{dx}{dt}, \quad (2.2)$$

where V is the input voltage, R is the coil resistance, L is the coil inductance and K_g is the back EMF constant. The coupling between the two equations is demonstrated in Fig. 4. Base-case values for k , K_f , K_g , L , m , R , as provided by Analog, are given in Table 1. Note that equations (2.1) and (2.2) also form the basis of other models for voice coil motors [4, 7]. Most of what follows focuses on equation (2.1), since it is believed that I can be controlled as required; however, there will be a need to return to equation (2.2) later.

Symbol	Meaning	Typical value
B	drag coefficient	$10^{-4} \text{ N s m}^{-1}$
k	spring stiffness	40 kg s^{-2}
I_{\max}	maximum current	0.1 A
K_f	magnetic force constant	0.09 N A^{-1}
K_g	back EMF constant	0.5 V s m^{-1}
L	coil inductance	$1 \times 10^{-6} \text{ H}$
m	mass of lens	$8 \times 10^{-5} \text{ kg}$
R	coil resistance	15 ohms
x_{\max}	maximum displacement	$2.5 \times 10^{-4} \text{ m}$

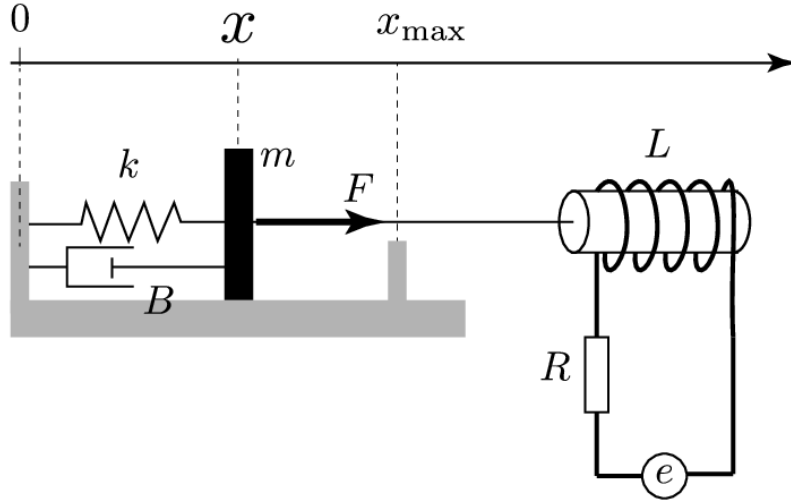


Figure 4: A schematic for the electromechanical model.

Table 1: Base-case model parameters

We will need initial conditions for equation (2.1). For these, we take

$$x(0) = x_0, \quad \dot{x}(0) = 0; \quad (2.3)$$

thus, the lens is initially stationary at some location x_0 , where $0 \leq x_0 < x_{\max}$, with x_{\max} as the maximum possible displacement.

Note that equation (2.1) ought to be fine-tuned to take better account of Fig. 3; more correctly,

$$m \frac{dx^2}{dt^2} + B \frac{dx}{dt} + kx = K_f (I - I_{nl}), \quad (2.4)$$

where I_{nl} is the current necessary to move the lens out of the so-called non-linear regime. Even this is an approximation, since x is not identically zero when this happens; for simplicity, we will simply set $I_{nl} = 0$. Furthermore, it makes most sense to consider the worst-case scenario which is when $x_0 = 0$, and the lens is required to move to $x = x_{\max}$. Observe also that (2.1) provides a consistency check on the model equations and the estimated model parameters: the worst-case scenario can only be achieved if

$$kx_{\max} < K_f I_{\max}; \quad (2.5)$$

from Table 1, $x_{\max} \lesssim 2.2 \times 10^{-4}$ m, indicating that it will not be possible to move the lens to x_{\max} if there is only 0.1 A at our disposal. Note that the worst-case scenario becomes more challenging if we use (2.4) as the basis of an inequality to replace (2.5):

$$kx_{\max} < K_f (I_{\max} - I_{nl}) \quad (2.6)$$

From Fig. 3, we have $I_{nl} \approx 0.025$ A for the case when the camera faces away from Earth, leading to $x_{\max} \lesssim 1.65 \times 10^{-4}$ m.

3 Nondimensionalization

For the purposes of this report, the following non-dimensional variables will suffice. We non-dimensionalise length with x_{\max} and time with t_{\max} ,

$$x = x_{\max} X, \quad t = t_{\max} \bar{t},$$

in which case (2.1) becomes, on dropping the bars,

$$\left(\frac{m x_{\max}}{t_{\max}^2}\right) \ddot{X} + \left(\frac{B x_{\max}}{t_{\max}}\right) \dot{X} + (k x_{\max}) X = F(t), \quad (3.1)$$

where $F(t) = K_f I(t)$ and the dot denotes rate of change with respect to non-dimensional time. This gives us a natural (inertial) force scale of

$$\left(\frac{m x_{\max}}{t_{\max}^2}\right) \sim 2 \times 10^{-4} \text{ N},$$

and so we define non-dimensional force by

$$F(t) = \left(\frac{m x_{\max}}{t_{\max}^2}\right) f(t).$$

We may then write (3.1) as

$$\alpha \ddot{X} + \beta \dot{X} + \gamma X = f(t), \quad (3.2)$$

where

$$\alpha = 1, \quad \beta = \frac{B t_{\max}}{m}, \quad \gamma = \frac{k t_{\max}^2}{m}.$$

The reason for introducing the apparently redundant α will be explained below when we consider the sensitivity of solutions to small perturbations in the physical parameters, which may occur as a result of the manufacturing process. Now, we have

$$\beta \sim 1/80, \quad \gamma \sim 50,$$

and equation (3.2) has homogeneous solutions of the form

$$\exp\left(\left[\frac{-\beta \pm i\sqrt{4\alpha\gamma - \beta^2}}{2\alpha}\right] t\right),$$

which implies a natural period of (damped) oscillations of approximately one in non-dimensional units; that is, the natural period is, more or less equal to the maximum time allowed to move the lens to a new position. Also, the fact that $\beta \ll 1$ confirms that the system is highly underdamped, which was already appreciated by Analog; this is unsurprising given the relatively stiff spring and the fact that the main damping mechanism appears to be air resistance.

4 Results

We present the results obtained so far in three parts. First, we demonstrate how it is possible to achieve oscillation-free shift. Then, we discuss the feasibility of digitization. Lastly, we consider the sensitivity of the results to the mass of the lens, the spring constant and the drag resistance.

4.1 Oscillation-free position shift

One means of eliminating oscillations is to ensure that when the lens is moved to its new position it arrives there with zero velocity and zero net force. To this end, we may prescribe a trajectory that achieves these goals and compute the force necessary to produce that trajectory. The issue then becomes whether or not it is possible to achieve that force in practice. The fact that we must produce the motion within approximately one period of the damped oscillator is all the better, as the lens will have no time to oscillate during the motion and so the applied force will not need to compensate for oscillations. There is no unique way to do this, and we consider several possibilities.

4.1.1 Cubic splines

One *simple* trajectory which achieves the goals above is given by one of the standard cubic spline basis functions, which satisfies

$$\frac{d^3 X}{dt^3} = 0, \quad X(0) = 0, \quad \dot{X}(0) = 0, \quad X(1) = 1, \quad \dot{X}(1) = 0;$$

this is given by

$$X(t) = (3 - 2t)t^2.$$

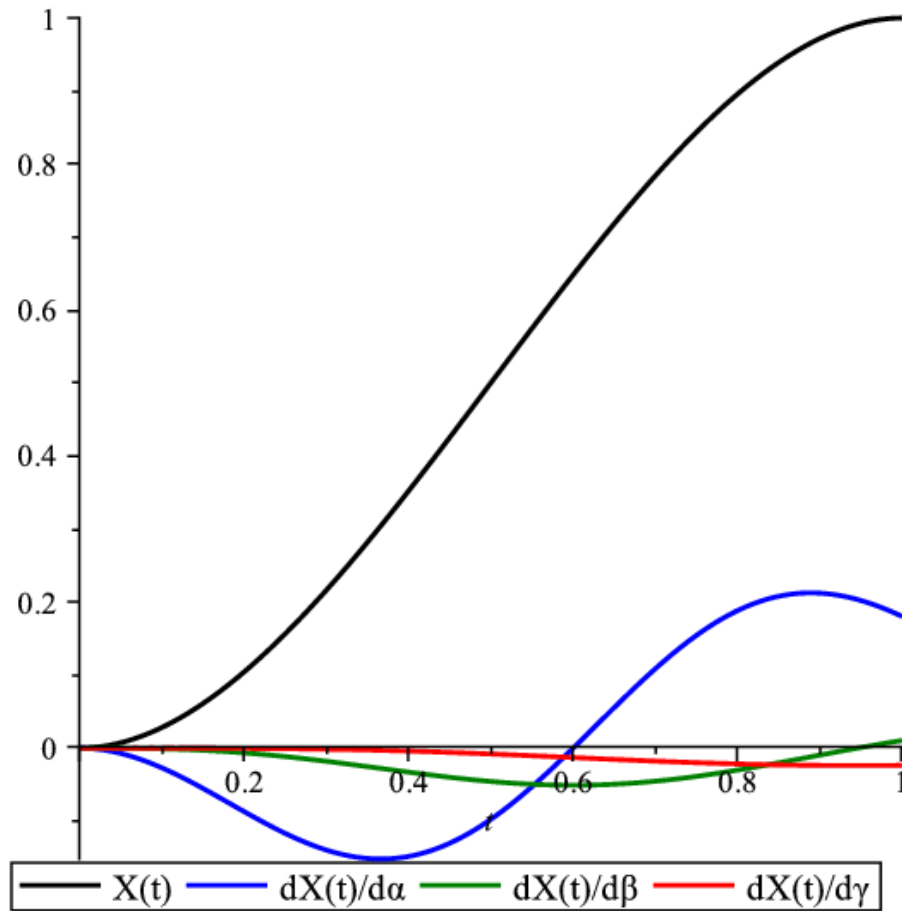


Figure 5: Prescribed cubic-spline displacement $X(t)$ and the sensitivities $\partial X(t)/\partial\alpha$, $\partial X(t)/\partial\beta$ and $\partial X(t)/\partial\gamma$ for the parameters given in Table 1.

and illustrated in Fig. 5. Substituting this into (3.2) gives a required force of

$$f(t) = 6 - \frac{477}{40}t + \frac{5997}{40}t^2 - 100t^3,$$

which is illustrated in Fig. 6.

There is, however, a problem here: the magnetic force $f(t)$ will not balance the spring force at $t = 1$ and so there will be a residual force pulling the lens from $X = 1$ back to $X = 0$. This will induce oscillations.

4.1.2 Quintic splines

There is, however, a simple way to avoid oscillations, which involves using higher order splines. For example, we can change the trajectory to a quintic that satisfies

$$\frac{d^6 X}{dt^6} = 0, \tag{4.1}$$

subject to the boundary conditions

$$\begin{aligned} X(0) = 0, \quad \dot{X}(0) = 0, \quad \ddot{X}(0) = 0, \\ X(1) = 1, \quad \dot{X}(1) = 0, \quad \ddot{X}(1) = 0. \end{aligned} \tag{4.2}$$

An example of this is shown in Fig. 7 which indicates $X(t)$ to be suitably behaved at $t = 1$ and beyond.

Nevertheless, as we shall see in Section 4.3, problems will still arise if there are any errors in the parameters: there will be oscillations in $x(t)$, particularly if the errors are in the mass or spring stiffness.

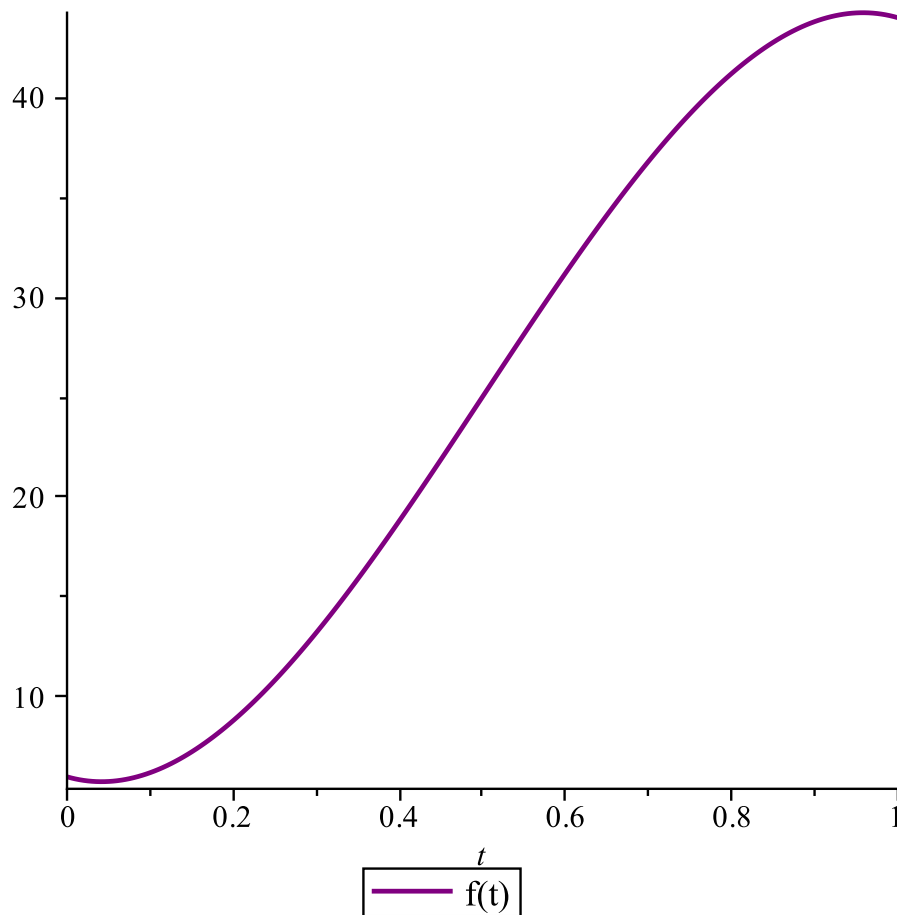


Figure 6: Non-dimensional force, $f(t)$, required to produce the cubic-spline trajectory shown in Figure 5, given the parameters in Table 1.

4.1.3 Hill functions

An alternative to splines are the *Hill functions*, $X_{A,T}^{(n)}$, given by

$$X_{A,T}^{(n)}(t) = \frac{At^n}{t^n + T}$$

where A , n and T are constants. Typically, $n = 2$ or 3 , and this will be sufficient to ensure that the initial conditions (2.3) are satisfied. These functions are shown in Fig. 8 and have a limiting value for $t \rightarrow \infty$ which is simply the constant A , whereas T is a measure of the point in time when the curve has maximal curvature and begins to approach the asymptote.

Fig. 9 shows, in the same plot, the solution $x(t)$ and the required forcing $f(t)$, which here has been normalized for convenience. One feature that is evident here, which was not evident when using splines, is that $f(t)$ mirrors $x(t)$ for larger values of T , but not as T decreases: for example, in the third plot of Fig. 9 has a local maximum and minimum before reaching its asymptotic value.

4.2 Digitalization

The results above assume that the forcing current and the displacement are both continuous functions of time; in reality, however, it is not possible to apply a continuously varying force - it has to be applied in discrete steps. Since Analog's CPU runs at 20 MHz, there should be no problem with digitalization in time, although the fact that the current will need to change in discrete steps may lead to concern: a digitalized profile current profile might lead to a vastly different displacement profile, as compared to that given by a continuous current profile. Fortunately, however, there should not be too much difference, essentially because the system is linear; hence, small changes to

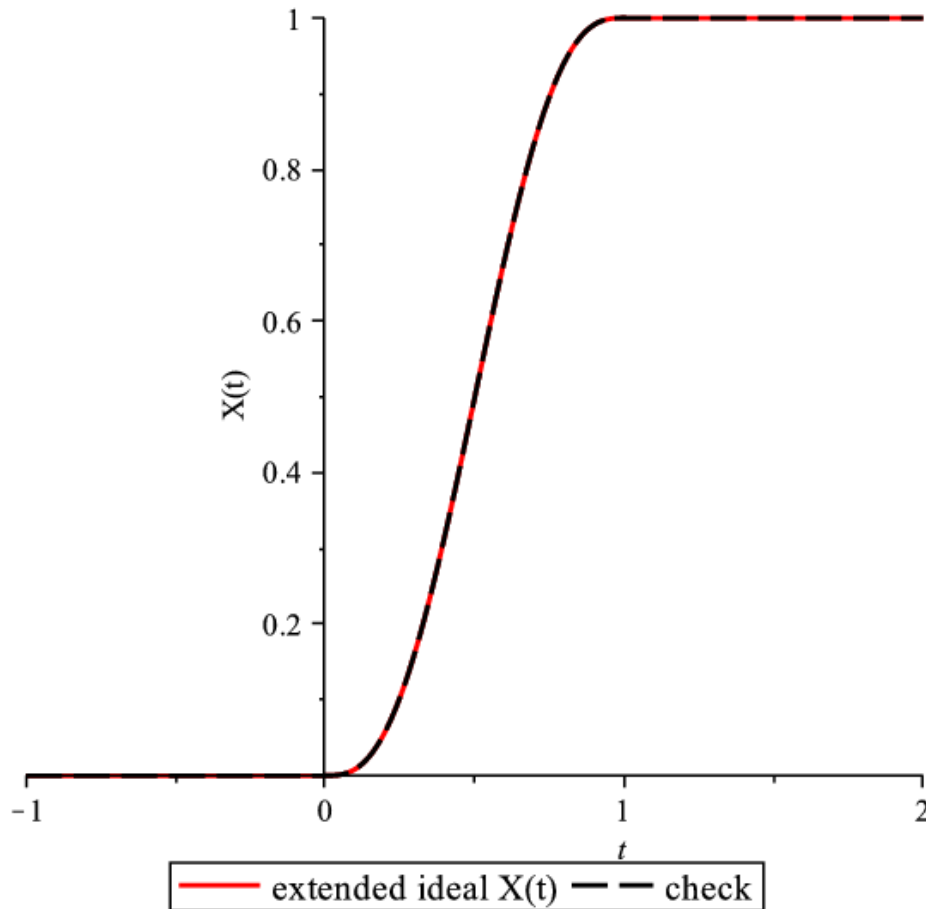


Figure 7: Quintic spline

$f(t)$ will produce small changes to $X(t)$ - a result that can be proved formally using a theorem on the continuous dependence on parameters (essentially Gronwall's inequality). An example of this is shown Fig. 10, which uses the forcing function in the third plot in Fig. 9 to attempt to recreate the displacement in that plot. Fig. 10 shows that, although not quite as smooth as the solution to a smooth force, the solution retains the qualitative features.

4.3 Sensitivities

If we proceed with the idea of prescribing a trajectory and computing the necessary force, then the computed force will depend on the values of α , β and γ above. If all lens mechanisms have *exactly* the same mass, resistance and spring constants, then it should work more or less perfectly, assuming the necessary force can be achieved. If, however, there are slight variations in any of these parameters, then the actual trajectory will be different from the intended trajectory and it is important to know how sensitive the actual trajectory will be to small variations in these parameters.

In non-dimensional variables, this amounts to computing the sensitivities

$$u = \frac{\partial X(t)}{\partial \alpha}, \quad v = \frac{\partial X(t)}{\partial \beta}, \quad w = \frac{\partial X(t)}{\partial \gamma}.$$

If these are large, then small variations in the manufacturing process will result in large changes in the achieved trajectories and the proposed method will be effectively useless.

In what follows we may assume that $f(t)$ has been computed using a reference system, and is therefore simply a prescribed function of time; manufacturing variation in any particular lens mechanism will not change it. If we differentiate (3.2) with respect to α , we find that $u = \partial X / \partial \alpha$ satisfies the problem

$$\alpha \ddot{u} + \beta \dot{u} + \gamma u = -\ddot{X}, \quad u(0) = 0, \quad \dot{u}(0) = 0.$$

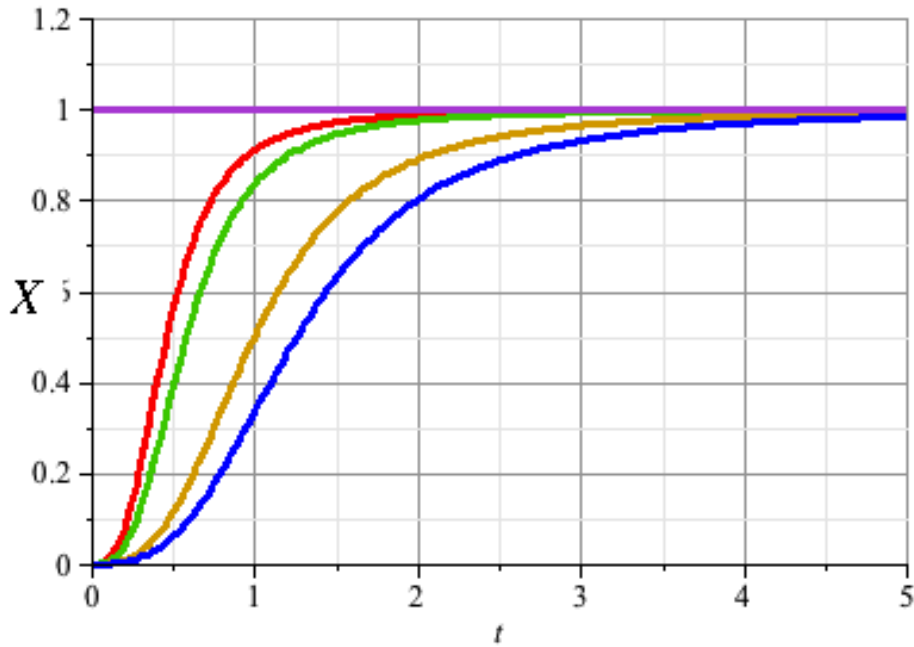


Figure 8: Hill functions for $n = 3$. The parameter A gives the asymptotic value, and T is a measure of the t value for which the curve begins to approach the asymptotic value. Shown are, for $A = 1$, curves with $T = 0.1, 0.2, 1.0$ and 2.0 .

As we are concerned with small variations in α , β and γ about their reference values, we may assume that these parameters correspond to the “reference” values used to determine $f(t)$ and that $X(t)$ corresponds to the prescribed trajectory. This problem is essentially the same as solving (3.2), for $X(t)$, with $f(t)$ set to $-\ddot{X}(t)$. The actual trajectory (assuming β and γ take their exact reference values) will be approximately

$$X(t) + u(t) \delta\alpha,$$

where again $X(t)$ is the desired trajectory and $\delta\alpha$ is the small variation in non-dimensional mass.

Similarly, the sensitivity of the actual trajectory to small variations in β may be determined using $v = \partial X / \partial \beta$, which may be obtained by solving the problem

$$\alpha \ddot{v} + \beta \dot{v} + \gamma v = -\dot{X}, \quad v(0) = 0, \quad \dot{v}(0) = 0,$$

and the sensitivity to small variations in γ is determined by $w = \partial X / \partial \gamma$;

$$\alpha \ddot{w} + \beta \dot{w} + \gamma w = -X, \quad w(0) = 0, \quad \dot{w}(0) = 0.$$

Note that with the cubic spline basis function for $X(t)$ given earlier, it is a simple matter to deduce that $v = \dot{w}$ and $u = \ddot{w}$. In addition to showing the cubic-spline trajectory $X(t)$, Fig. 5 also shows the sensitivities $u(t)$, $v(t)$ and $w(t)$. These sensitivities appear to be reasonable, although it is difficult to be certain without knowing the manufacturing tolerances for m , B and k ; the force required to produce this reference trajectory, given the parameters in Table 1, has already been shown in Fig. 6. The trajectory which is achieved if this force is applied to a system with slightly perturbed (by about $\pm 10\%$) parameters is shown in Fig. 11 and is consistent with the sensitivities shown in Fig. 5.

Lastly, in Figs. 12-15, we show how the quintic-spline trajectory is affected by variations in the model parameters. Evident here, and as mentioned earlier, is the fact that, even though Fig. 7 showed that it was possible to achieve oscillation-free displacement with quintic splines, variations of as little as 5% in the model parameters can lead to sizeable oscillations in the displacement as it approaches a steady state.

5 Conclusion

This report has considered an electromechanical model for the operation of a voice coil motor in a mobile phone camera, with the aim of optimizing how a lens can be moved to a desired focusing motion; only the mechanical part

of the model was considered in any great depth, however. Although we have developed a methodology for optimizing lens shift, there is some concern about the model parameters that were at our disposal. Central to the model is the value of the estimated magnetic force constant, K_f : its value determines how far it is actually possible to move the lens, but it appears that, from the value given, it would not be possible to shift the lens through the displacements desired. Furthermore, experiments at Analog have also estimated the value of the back EMF constant, K_g , to be roughly five times greater than K_f , even though we have presented two theoretical arguments, in Appendices A and B, that show that $K_f = K_g$; these conclusions are supported by readily-available data for voice coil motors (e.g. see <http://www.pwr-con.com/>). It will therefore be necessary to understand exactly how Analog are determining these constants, as they are central to any future modelling effort.

This report did not tackle the so-called non-linear problem. The only way that it is possible to detect when the magnetic current overcomes the pre-stress in the spring is via the back EMF induced when the lens starts moving. Whilst it is difficult to give a sensible suggestion for this, one possibility could be to compute the onset of the non-linear region while doing an initial focus by looking for the discontinuity in the slope of the voltage versus current curve. Ideally, this should be done without using numerical differentiation, as this is a notoriously unstable process.

Acknowledgments

W. T. Lee, E. Murphy and M. Vynnycky acknowledge the support of the Mathematics Applications Consortium for Science and Industry (www.macsi.ul.ie) funded by the Science Foundation Ireland Mathematics Initiative Grant 06/MI/005.

Appendix A: Energy equation

Multiplying the momentum equation (2.1) by \dot{x} , the circuit equation (2.2) by I , and adding leads to the equation

$$\underbrace{IV}_{\text{supplied power}} = \underbrace{I^2 R + B\dot{x}^2}_{\text{dissipation}} + \underbrace{\frac{d}{dt} \left(\frac{1}{2} m \dot{x}^2 + \frac{1}{2} k x^2 + \frac{1}{2} L I^2 \right)}_{\text{rate of change of stored energy}} + (K_g - K_f) I \dot{x}. \quad (\text{A1})$$

The K_f and K_g terms are responsible for the conversion of magnetic energy into kinetic energy and vice versa, a process that must leave the total energy unchanged. The last term involving $K_g - K_f$ is therefore spurious, and we require $K_g = K_f$. The two coefficients are commonly quoted in units of N/A for K_f , and Vs/m for K_g , but these two apparently different units are identical because $V=W/A$.

Equation (A1) then becomes the expected energy equation that relates the change in the system's stored energy to the power IR supplied in the circuit, and to the dissipation through mechanical friction and Ohmic heating. The stored energy comprises kinetic, elastic, and magnetic contributions.

Appendix B: Determining K_f and K_g from Maxwell's equations

Following Ampère, we model the permanent magnets as a set \mathcal{P} of loops through which a current J flows. The supplied current I flows through the coil \mathcal{C} . Ampère's force law gives the magnetic force exerted by the current-carrying loop \mathcal{C} on the currents flowing in the permanent magnet \mathcal{P} . Using page 178 of [3], this force is

$$\mathbf{F} = \frac{\mu_0}{4\pi} \oint_{\mathcal{P}} \oint_{\mathcal{C}} \frac{\mathbf{r} - \mathbf{p}}{|\mathbf{r} - \mathbf{p}|^3} d\mathbf{r} \cdot d\mathbf{p}, \quad (\text{B1})$$

where μ_0 is the magnetic permeability, $d\mathbf{r}$ and $d\mathbf{p}$ are infinitesimal line elements on the curves \mathcal{C} and \mathcal{P} , respectively. The axial component $\mathbf{F} \cdot \hat{\mathbf{x}}$ is thus related to the current I by

$$\mathbf{F} \cdot \hat{\mathbf{x}} = K_f I, \quad (\text{B2})$$

where

$$K_f = \frac{\mu_0}{4\pi} \oint_{\mathcal{P}} \oint_{\mathcal{C}} \hat{\mathbf{x}} \cdot \frac{\mathbf{r} - \mathbf{p}}{|\mathbf{r} - \mathbf{p}|^3} d\mathbf{r} \cdot d\mathbf{p}. \quad (\text{B3})$$

Meanwhile, the back EMF is determined by integrating Faraday's law,

$$\frac{\partial \mathbf{B}}{\partial t} + \nabla \times \mathbf{E} = 0, \quad (\text{B4})$$

around the coils \mathcal{C} . Writing $\mathbf{B} = \nabla \times \mathbf{A}$ using a vector potential \mathbf{A} , the back EMF is given by

$$\Phi = \oint_{\mathcal{C}} \mathbf{E} \cdot d\mathbf{r} = -\frac{d}{dt} \oint_{\mathcal{C}} \mathbf{A} \cdot d\mathbf{r},$$

The time derivative of the integral of \mathbf{A} around the material curve \mathcal{C} undergoing rigid-body motion with velocity \mathbf{U} is, using page 133 of [1],

$$\Phi = -\oint_{\mathcal{C}} \left(\frac{\partial}{\partial t} + \mathbf{U} \cdot \nabla \right) \mathbf{A} \cdot d\mathbf{r}.$$

Combining these expressions, the back EMF generated solely by a rigid-body motion, $\mathbf{U} = U\hat{\mathbf{x}}$, of the magnets relative to the coil in the axial direction is

$$\begin{aligned} \Phi &= -\frac{\mu_0 J}{4\pi} \frac{d}{dt} \oint_{\mathcal{C}} \oint_{\mathcal{P}} \frac{1}{|\mathbf{r} - \mathbf{p}|} d\mathbf{p} \cdot d\mathbf{r} \\ &= -\frac{\mu_0 J}{4\pi} \oint_{\mathcal{C}} \oint_{\mathcal{P}} U\hat{\mathbf{x}} \cdot \nabla_{\mathbf{r}} \left(\frac{1}{|\mathbf{r} - \mathbf{p}|} \right) d\mathbf{p} \cdot d\mathbf{r} \\ &= \frac{\mu_0 U J}{4\pi} \hat{\mathbf{x}} \cdot \oint_{\mathcal{C}} \oint_{\mathcal{P}} \frac{\mathbf{r} - \mathbf{p}}{|\mathbf{r} - \mathbf{p}|^3} d\mathbf{p} \cdot d\mathbf{r} \\ &= K_g U. \end{aligned} \tag{B5}$$

Comparing (B2) and (B5), we see that the coefficients K_f and K_g in the relations $\mathbf{F} \cdot \hat{\mathbf{x}} = K_f I$ and $\Phi = K_g U$ are defined by the same double integral, and are therefore equal, as was concluded in Appendix A.

References

- [1] G. K. Batchelor. *An Introduction to Fluid Dynamics*. Cambridge University Press, Cambridge, 1967.
- [2] J. D. Hsu, C. L. Tsai, and Y. Y. Tzou. Design and implementation of a voice-coil motor servo control ic for auto-focus mobile camera applications. In *Proceedings of 2007 IEEE 38th Annual Power Electronics Specialists Conference, Florida, USA*, pages 1357–1362, June 2007.
- [3] J. D. Jackson. *Classical Electrodynamics*. Wiley, New York, 3rd edition, 1999.
- [4] S.-K. Lin, T.-C. Lee, and C.-L. Tsai. Application of sliding mode control to friction compensation of a mini voice coil motor. In *?*, pages 203–218. InTech Open Access.
- [5] S. K. Lin, C. M. Wang, and S. J. Wang. Design and implementation of anti-handshaking position control for a voice coil motor. *J. Appl. Phys.*, 103:Art. No. 07F128, 2008.
- [6] S. K. Lin, C. M. Wang, and S. J. Wang. Design of a voice coil motor used in the focusing system of a digital video camera. *IEEE Transactions on Magnetics*, 41:3979–3981, 2005.
- [7] C.-L. Tsai, T.-C. Lee, and S.-K. Lin. Friction compensation of a mini voice coil motor by sliding mode control. In *IEEE International Symposium on Industrial Electronics 2009, Seoul, Korea*, pages 609–614, 5-8 July 2009.

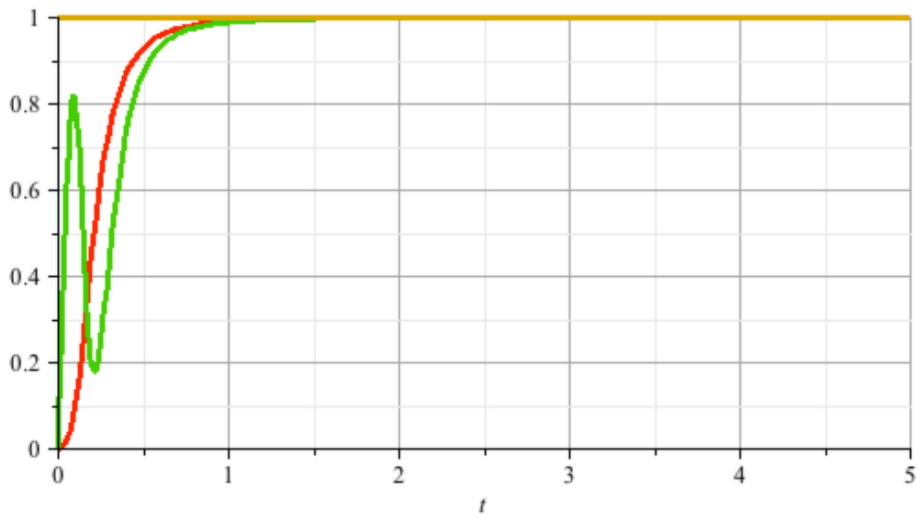
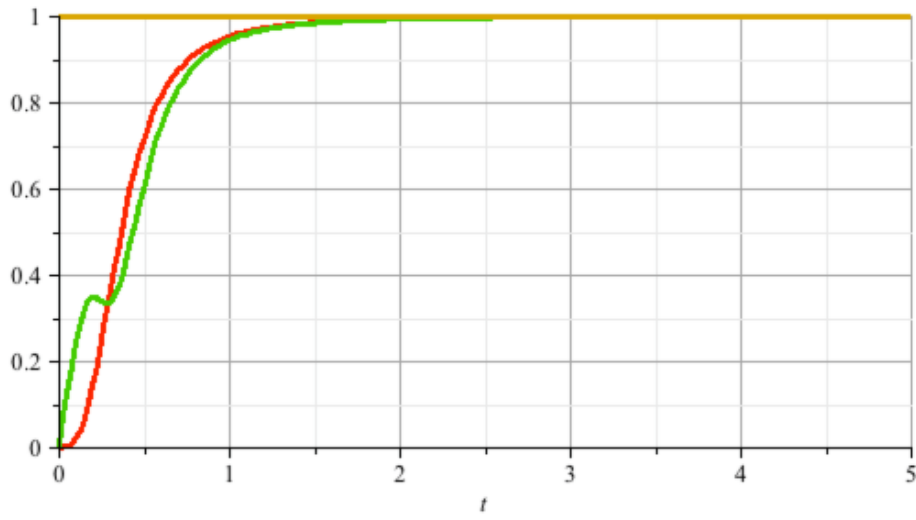
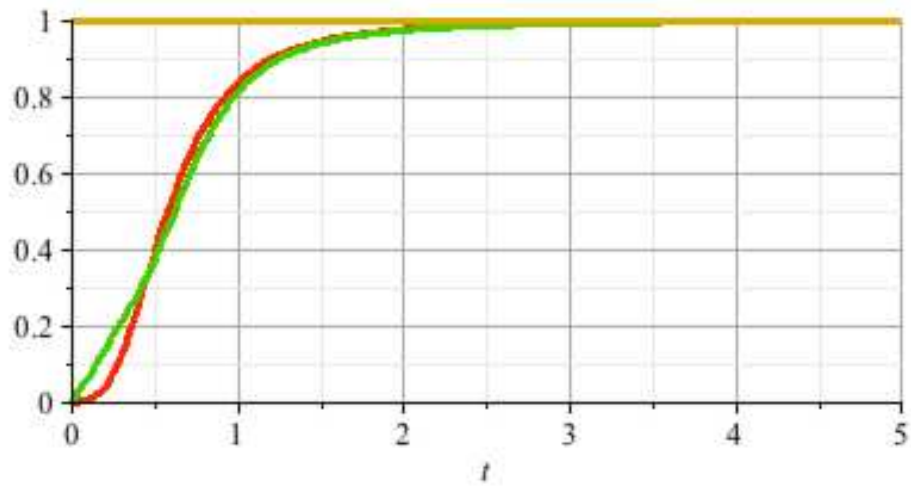


Figure 9: Time evolution of three solutions to (3.2). The curves are for $X(t)$, and the green curves are for normalized $f(t)$.

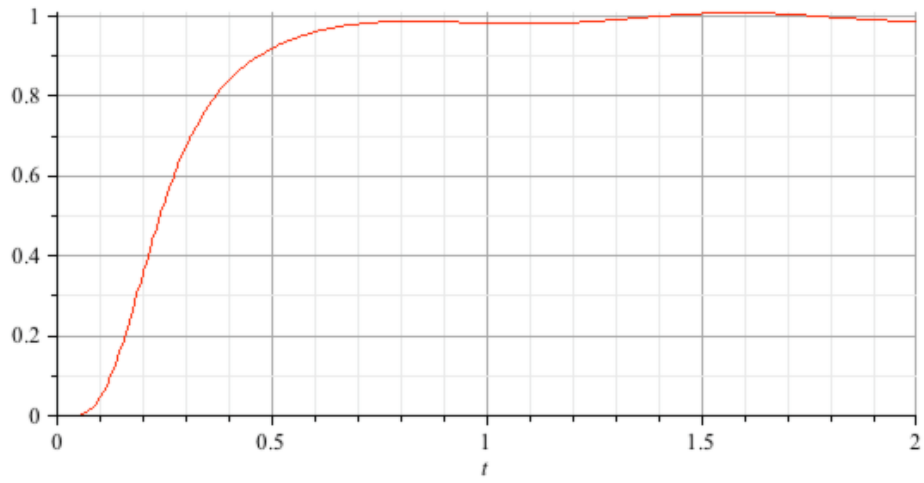


Figure 10: Time evolution of the displacement when using the digitalized form of the force from the third plot in Fig. 9 to find the solution to equation (3.2)

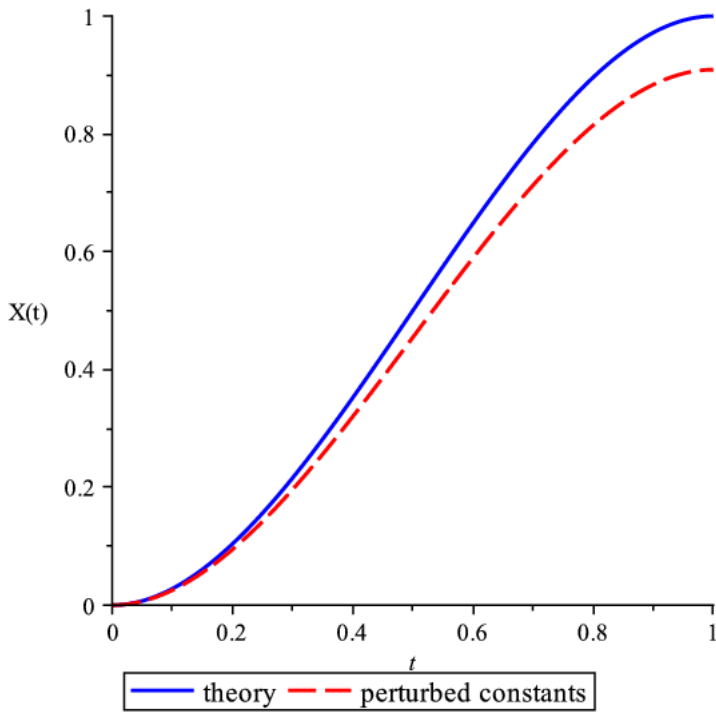


Figure 11: Comparison of the cubic-spline trajectory and the trajectory achieved if the non-dimensional force, $f(t)$, shown in Figure 6 is applied to (3.2) with perturbed values $\hat{\alpha} = 1.1 \alpha$, $\hat{\beta} = 0.9 \beta$ and $\hat{\gamma} = 1.1 \gamma$.

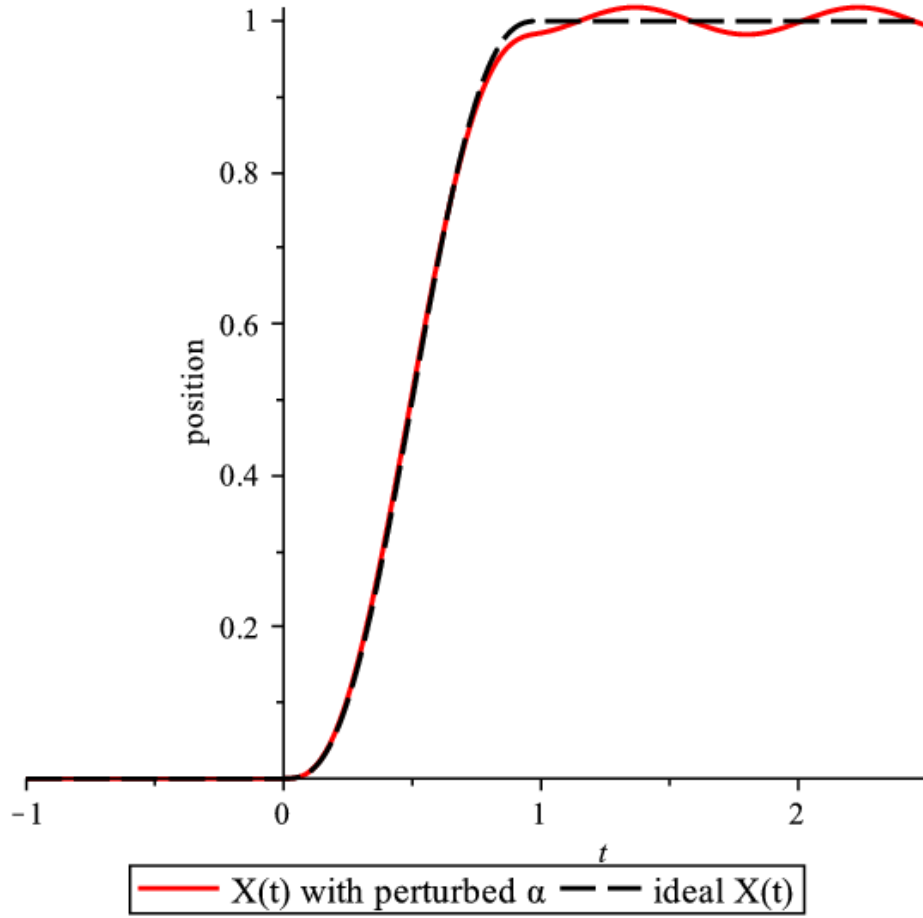


Figure 12: Comparison of the quintic-spline trajectory and the trajectory achieved if the non-dimensional force, $f(t)$, shown in Figure 6 is applied to equation (3.2) with the perturbed values $\hat{\alpha} = 1.05 \alpha$.

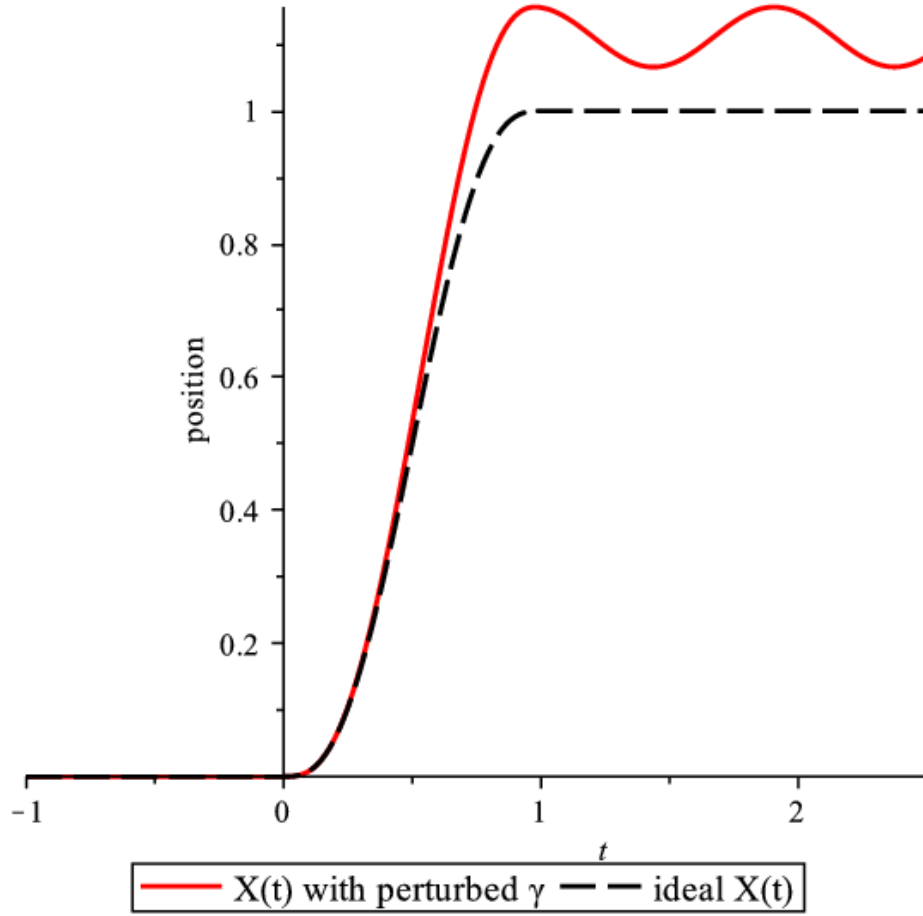


Figure 13: Comparison of the quintic-spline trajectory and the trajectory achieved if the non-dimensional force, $f(t)$, shown in Figure 6 is applied to equation (3.2) with the perturbed values $\hat{\gamma} = 1.05 \gamma$.

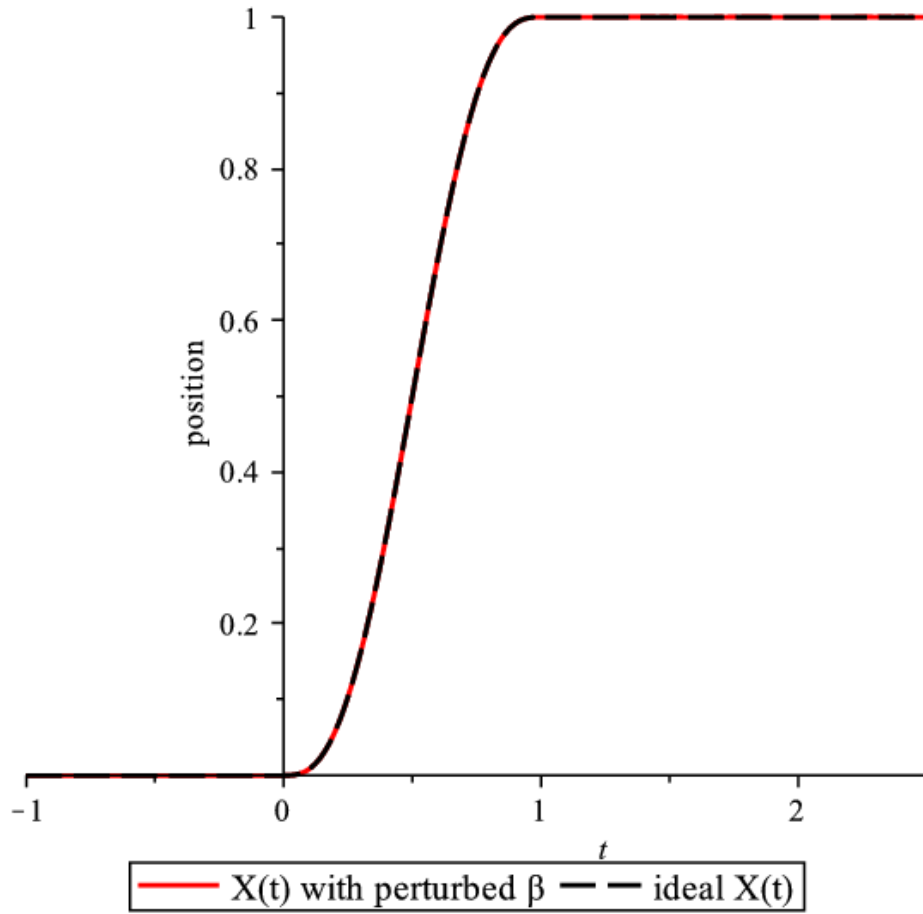


Figure 14: Comparison of the quintic-spline trajectory and the trajectory achieved if the non-dimensional force, $f(t)$, shown in Figure 6 is applied to equation (3.2) with the perturbed values $\hat{\beta} = 1.1\beta$.

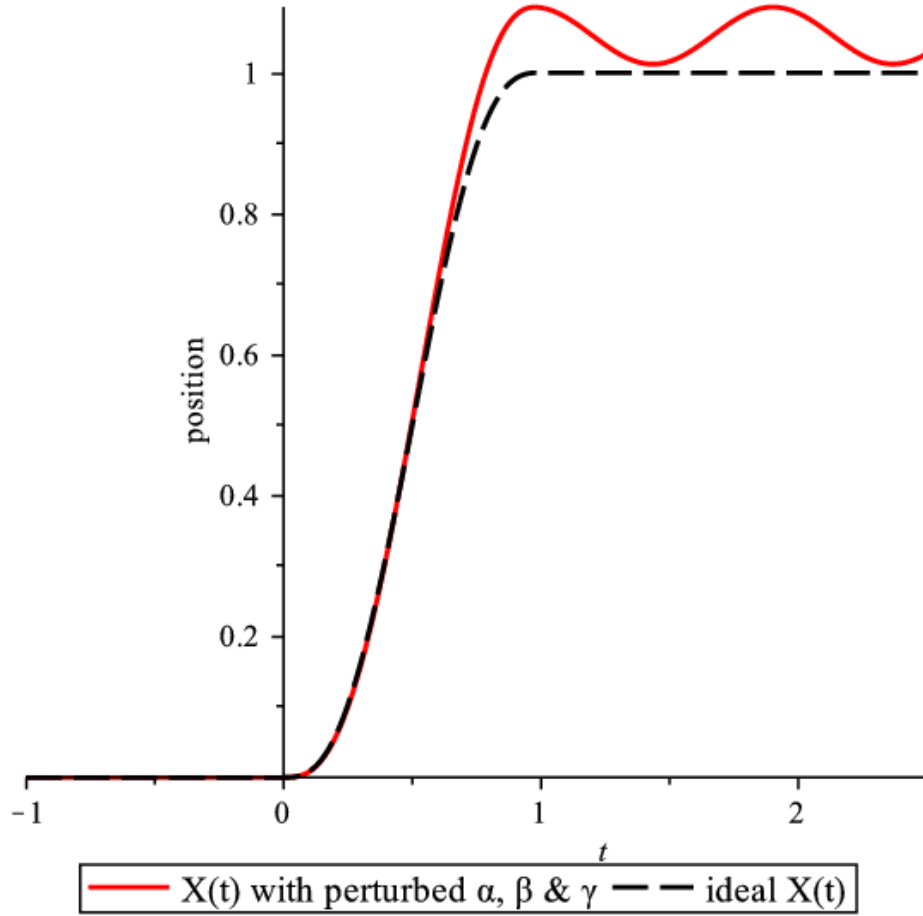


Figure 15: Comparison of the quintic-spline trajectory and the trajectory achieved if the non-dimensional force, $f(t)$, shown in Figure 6 is applied to equation (3.2) with the perturbed values $\hat{\alpha} = 1.05 \alpha$, $\hat{\beta} = 1.05 \beta$ and $\hat{\gamma} = 1.05 \gamma$.